J. Mech. Phys. Solids 191 (2024) 105755

Contents lists available at ScienceDirect

Journal of the Mechanics and Physics of Solids

journal homepage: www.elsevier.com/locate/jmps

Initiation and arrest of cracks from corners in multi-chip semiconductor devices

Guodong Nian [a], Yu-Sheng Lin [b], Jia-Ming Yang [b], Sammy Hassan [a], Jyun-Lin Wu [b], Sherwin Tang [b], Jun He [b], Joost J. Vlassak [a], Zhigang Suo [a,*]

[a] John A. Paulson School of Engineering and Applied Sciences, Harvard University, Cambridge, MA 02138, USA
[b] Quality and Reliability, Taiwan Semiconductor Manufacturing Company, Ltd., Hsinchu, Taiwan

ARTICLE INFO

Keywords:
Crack initiation
Crack arrest
Corner
Interfacial toughness
Semiconductor devices

ABSTRACT

A contemporary semiconductor device often contains multiple chips. Corners of the chips concentrate stress, and are principal sites to initiate failure. Here we propose to characterize the corners using a double cantilever beam, in which two silicon beams sandwich a row of chips. As the two beams are pulled open, a crack initiates at the corner of a chip, and runs unstably on the interface between the chip and a beam. The crack may or may not arrest, depending on various experimental conditions. We calculate energy release rate as a function of crack length by using a combination of finite element method and an analytical solution of the singular field around a corner. At a fixed applied displacement, the energy release rate is low for a short crack, peaks for a crack of intermediate length, and drops for a long crack. This non-monotonic behavior explains how a crack initiates, grows unstably, and possibly arrests. If the crack does arrest, as the two beams open further, the crack grows stably. We relate the initiation and arrest of the crack to machine compliance, specimen geometry, and flaw size. The force at which the crack initiates can be used to characterize the manufacturing process, whereas the stable growth of the crack can be used to measure interfacial toughness. It is hoped that this work will aid the development of multi-chip semiconductor devices.

1. Introduction

A semiconductor device today often integrates multiple chips (Lau, 2022). This architecture of three-dimensional integrated circuits (3D ICs) is compact, reduces power consumption, and increases data exchange rates. 3D ICs have enabled applications including artificial intelligence, high-performance computing, and human-machine interfaces.

Conspicuous in 3D ICs are corners, where edges of chips meet the surface of a substrate. During fabrication and operation of a device, dissimilar materials are integrated in sequence, at various temperatures. The process of integration and change in temperature induce stresses. The stresses concentrate at the corners, from which cracks often initiate and grow (Chen et al., 2021; Rabie et al., 2021). Cracks reduce the yield of devices during fabrication, and lower the reliability of them during operation (Lu et al., 2023).

Here we propose an approach to characterize corners. A model structure involves a row of chips sandwiched between two cantilever beams (Fig. 1a). In the drawing, for example, the first two chips are bonded to the bottom beam but not the top beam, and all the other chips are bonded to both beams. Denote the initial non-bonded beam length by b_0, the length of a crack emanating from a

* Corresponding author.
E-mail address: suo@seas.harvard.edu (Z. Suo).

https://doi.org/10.1016/j.jmps.2024.105755
Received 30 March 2024; Received in revised form 24 June 2024; Accepted 25 June 2024
Available online 27 June 2024

corner by a, the total crack length by b, the thickness of the chip by h, the thickness of the beam by H, the length of the chip by l_{chip}, and the machine compliance by C_{m}. The two beams are pulled open by a tensile tester at a fixed speed. The force P is recorded as a function of the displacement Δ (Fig. 1b). Initially, the force increases with the displacement linearly. At a critical displacement Δ_{c}, the force peaks at P_{c}, and a crack initiates from a corner of a chip. The crack runs on an interface between the chip and a beam. The crack speed is much faster than the speed of the crosshead of the tensile tester. Consequently, as the crack grows, the force drops precipitously, while the tensile tester does not have time to increase the displacement appreciably. Then the crack arrests. As the tensile tester increases the displacement further, the crack grows stably and the force decreases gradually.

The peak force at which the crack initiates characterizes the manufacturing process. A process that produces smaller flaws at the corner leads to a larger peak force. The length at which the crack arrests, as well as subsequent stable growth of the crack, characterizes interfacial toughness. This paper answers two questions: Why does a crack initiated from a corner grow unstably? Under what conditions does the crack arrest before running to the other corner of the chip? We interpret initiation, unstable growth, and arrest of the crack in terms of non-monotonic dependence of the energy release rate on the crack length (Section 2). When the crack is long compared to the thickness of the chip, the energy release rate coincides with the classical result for a double cantilever beam (Section 3). When the crack is short compared to the thickness of the chip, the energy release rate is obtained by a combination of finite element simulations and an analytical solution of the singular field around a corner (Section 4). We obtain the energy release rate as a function of the crack length. Using this function, we analyze the conditions of crack initiation and arrest (Section 5). The peak force leads to an estimate of the flaw size, and the stable crack growth provides a means to determine interfacial toughness experimentally. It is hoped that this work will aid the development of semiconductor devices of emerging architectures in which corners are ubiquitous.

2. Initiation, unstable growth, and arrest of a crack

For a crack emanating from a corner, the energy release rate, G, is a function of two variables: the length a of the crack, and the

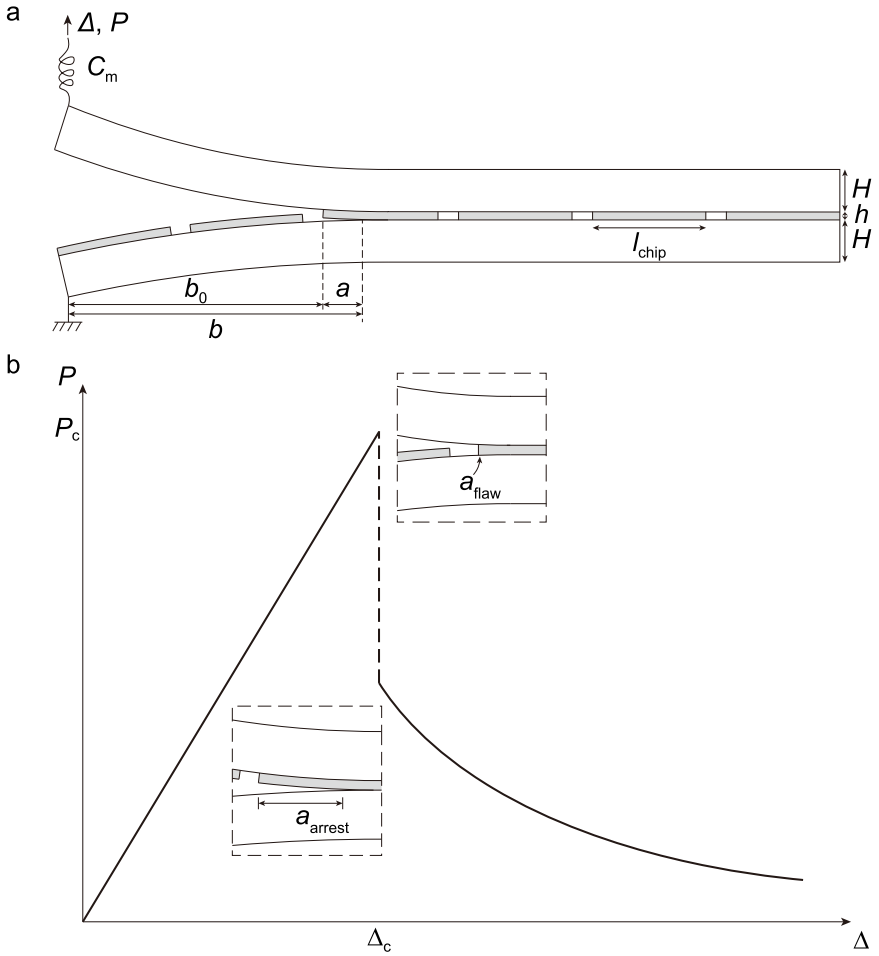

Fig. 1. Initiate and arrest a crack from a corner. (a) A double cantilever beam sandwiches several chips. A crack of length a lies on the interface between a chip and a beam. (b) As a beam is pulled by a force P, the crack initiates at a corner, runs unstably on the interface, and arrests before reaching the other corner. Marked on the force-displacement curve are two states: crack initiation and crack arrest.

displacement Δ applied by the tensile tester. The tensile tester is programmed to apply the displacement at a constant speed. At a given time, the displacement is at a certain value, and the energy release rate is a non-monotonic function of the crack length. As $a \to 0$, the energy release rate vanishes. When the crack is short compared to the thickness of the chip, $a << h$, the energy release rate increases with the crack length. When the crack is long compared to the thickness of the chip, $a >> h$, the energy release rate coincides with that of a double cantilever beam. At a constant displacement, the energy release rate of the double cantilever beam is known to decrease as the crack length increases. These limits for a short crack and a long crack indicate that, at a constant displacement, the energy release rate is a non-monotonic function of the crack length.

Sketch the function $G(\Delta, a)$ on the G-a plane for three constant displacements (Fig. 2). As discussed above, at a constant displacement, G is a non-monotonic function of a. For any given crack length a, the larger the displacement Δ, the larger the energy release rate G. Mark the toughness G_c as a horizontal dashed line. Assume that a small crack-like flaw preexists at the corner, and mark the length of the flaw, a_{flaw}, as a vertical dashed line. When the displacement Δ is small, the energy release rate is below the toughness, $G(\Delta, a_{\text{flaw}}) < G_c$, so the flaw remains dormant. When the energy release rate equals the toughness, namely, when the line $G = G_c$ intersects the line $a = a_{\text{flaw}}$, the flaw begins to grow as a crack along the interface between the chip and the substrate. Thus, the critical displacement Δ_c is determined by

$$G\left(\Delta_c, a_{flaw}\right) = G_c. \tag{1}$$

Because the tensile tester is programmed to apply the displacement at a constant speed, the displacement is nearly unchanged in a short time. At the nearly constant displacement, as the crack grows, the energy release rate exceeds the toughness, $G > G_c$. Consequently, the crack grows unstably until the curve intersects with the line $G = G_c$ again:

$$G(\Delta_c, a_{arrest}) = G_c. \tag{2}$$

This intersection determines the length at which the crack arrests a_{arrest}.

Thus, at the critical displacement Δ_c, the non-monotonic $G(\Delta_c, a)$ curve intersects the horizontal dashed line $G = G_c$ at two points, corresponding to two states: crack initiation and crack arrest. The state of crack initiation is unstable because the slope of the $G(\Delta_c, a)$ at crack initiation is positive. The state of crack arrest is stable because the slope of the $G(\Delta_c, a)$ at crack arrest is negative. Between crack initiation and arrest, as the speed of the crack is much faster than the speed of the crosshead of the tensile tester, the displacement remains nearly unchanged at the critical value. Subsequently, as the tensile tester increases the displacement, the crack grows stably.

3. Global energy release rate

The thickness of the chip is small compared to the thickness of the beam and the length of the chip, $h << H$ and $h << l_{\text{chip}}$. Let r be the distance from the crack tip. An annulus exists, $h << r << H$, in which the stress field is well represented by the square root singularity of a crack in a linear elastic body. In this annulus, the amplitude of the load is represented by an energy release rate, which we call the global energy release rate, G_∞ (Fig. 3a). Near the crack tip, the stress field is in general influenced by the presence of the chip. The amplitude of the load is represented by another energy release rate, which we call the local energy release rate, G (Fig. 3b).

For the double cantilever beam, the global energy release rate takes the form (Wiederhorn et al., 1968):

$$G_\infty = \frac{12P^2}{EW^2H}\left[\frac{b}{H} + 0.677\right]^2 \tag{3}$$

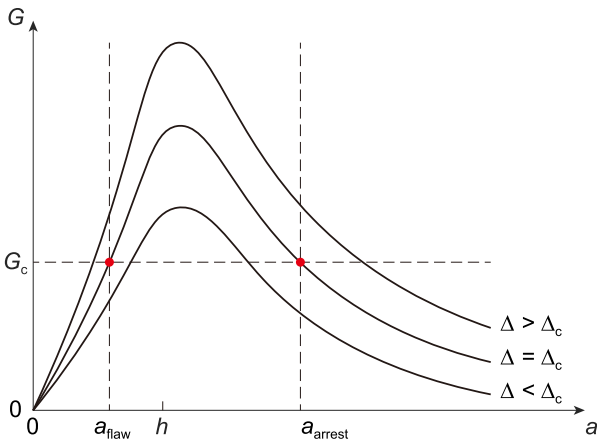

Fig. 2. The energy release rate as a function of two variables, $G(\Delta, a)$, is plotted on the G-a plane. The horizontal dashed line represents the toughness G_c. One vertical dashed line represents the length of a crack-like flaw, a_{flaw}, and the other vertical dashed line represents the length at which the crack arrests, a_{arrest}.

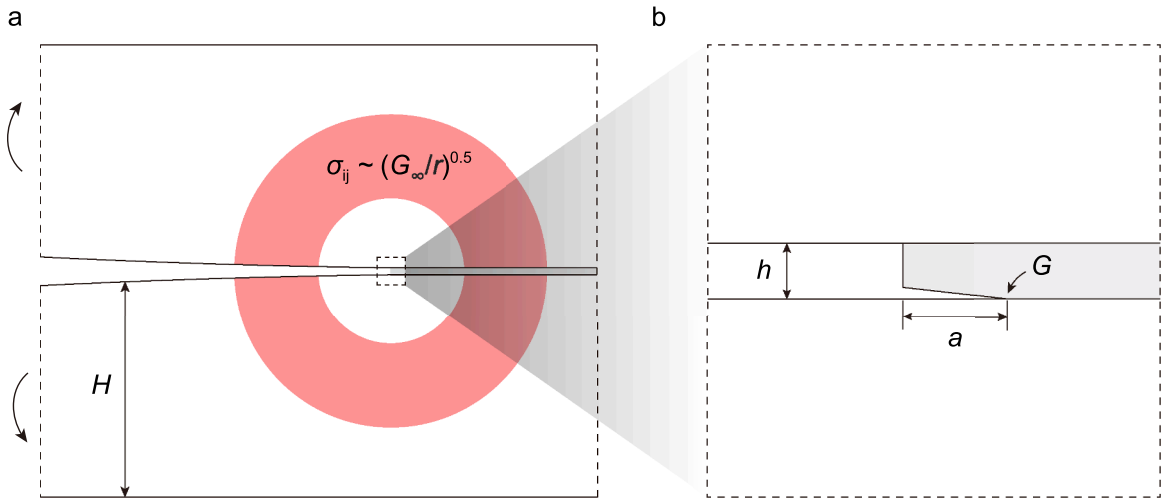

Fig. 3. A crack emanates from a corner. (a) In the double cantilever beam, an annulus exists, $h << r << H$, within which the stress field is described by the square root singularity. In this annulus, the applied load communicates to the crack tip via the global energy release rate G_∞. (b) Near the crack tip, the stress field is in general influenced by the presence of the chip. The field at the crack tip is scaled by the local energy release rate G.

where $b = b_0 + a$ is the total crack length (Fig. 1a), W is the beam width, and $E' = E/(1\text{-}\nu^2)$ is the plane strain modulus. We use the same modulus (E) and Poisson's ratio (ν) for both the beam and the chip, as their main component is silicon.

Because the tensile tester applies the displacement, we next derive the global energy release rate as a function of the displacement. Assume that the system is linearly elastic, $\Delta = CP$, where C is the compliance of the system. The compliance is a function of the total crack length. The longer the crack, the longer the non-bonded beams, and the larger the compliance. The elastic energy stored in the system is a function of the force and the total crack length, $U(P, b) = P^2C(b)/2$. Recall the definition of the energy release rate $G_\infty = \partial U(P, b)/\partial bW$ (Rivlin and Thomas, 1953). Thus, $G_\infty = (\partial C/\partial b)P^2/2W$. By inserting Eq. (3), we obtain that

$$\frac{\partial C}{\partial b} = \frac{24}{E'WH}\left[\frac{b}{H} + 0.677\right]^2. \tag{4}$$

By integration, we obtain that

$$C = C_m + \frac{8}{E'W}\left[\left(\frac{b}{H}\right)^3 + 2.031\left(\frac{b}{H}\right)^2 + 1.375\frac{b}{H}\right] \tag{5}$$

where the first term represents the machine compliance and the second term represents the specimen compliance. The machine compliance is often measured using a standard sample with known compliance (Blackman and Kinloch, 2001).

By substituting Δ/C for P in Eq. (3), we obtain that

$$G_\infty = \frac{3\Delta^2 E'}{16H}\frac{\left(\frac{b}{H} + 0.677\right)^2}{\left[c_m + \left(\frac{b}{H}\right)^3 + 2.031\left(\frac{b}{H}\right)^2 + 1.375\frac{b}{H}\right]^2} \tag{6}$$

where the machine compliance is normalized as $c_m = C_m E'W/8$.

Eqs. (5) and (6) are commonly used in the experimental measurement of toughness. Consider a crack that initiates from a chip-substrate corner, grows unstably, and arrests before reaching the other corner. As the tensile tester increases the displacement further, the crack grows stably. Assume that the crack tip is far away from either corner. The thickness of the chip is small and has a negligible effect on the energy release rate. In an experiment, directly measuring the crack length is often inconvenient, but the compliance is readily obtained from the force-displacement curve. From the measured compliance, Eq. (5) is used to determine the total crack length b, and Eq. (6) is used to determine the toughness.

4. Local energy release rate

The local energy release rate takes the following form

$$G = G_\infty f\left(\frac{a}{h}\right) \tag{7}$$

where f is a dimensionless function of the normalized crack length a/h. The local energy release rate is in general different from the global energy release rate. The physical nature of the difference is a geometric effect of the chip corner.

When the crack length is small compared to the chip thickness, $a << h$, the corner singularity governs the short crack, and the overall specimen geometry scales the local energy release rate G only through G_∞. This scenario is called the short-crack limit. We next determine G-a relation for the short-crack limit.

Recall the stress field at a corner in a linear elastic body in the absence of crack (Fig. 4a). The stress field is singular at the corner (Williams, 1952):

$$\sigma_{ij}(r,\theta) = k_1 r^{-\lambda_1}\Sigma_{ij}^1(\theta) + k_2 r^{-\lambda_2}\Sigma_{ij}^2(\theta) \tag{8}$$

where (r, θ) represent polar coordinates of material particles. Associated with the two modes of the singularity are two exponents λ_1 and λ_2, two intensity factors k_1 and k_2, and two angular distributions $\Sigma_{ij}^1(\theta)$ and $\Sigma_{ij}^2(\theta)$. Both exponents are functions of the angle ψ (Fig. 4b). When $\psi = 0$, the corner becomes a crack, both modes have the same exponent $\lambda_1 = \lambda_2 = 0.5$. When $\psi > 0$, the exponent splits into two distinct values, $\lambda_1 < \lambda_2 < 0.5$. The split singularities have been discussed in a previous paper (Liu et al., 1999).

In the absence of a crack, the thickness of the chip, h, is the only length scale of the local geometry. The overall geometry and applied load enter through the global energy release, G_∞. Linearity and dimensional considerations dictate that the stress intensity factors of the corner take the form:

$$k_1 = \kappa_1 h^{\lambda_1 - \frac{1}{2}}\sqrt{G_\infty E'}, \tag{9a}$$

$$k_2 = \kappa_2 h^{\lambda_2 - \frac{1}{2}}\sqrt{G_\infty E'} \tag{9b}$$

where κ_1 and κ_2 are coefficients linked to the split singularities at the corner.

For a short crack emanating from the corner, $a << h$, the stress intensity factors of the crack, K_I and K_{II}, are linear in the stress intensity factors of the corner, k_1 and k_2. Dimensional considerations dictate the following form:

$$K_I = c_{11}k_1 a^{\frac{1}{2}-\lambda_1} + c_{12}k_2 a^{\frac{1}{2}-\lambda_2}, \tag{10a}$$

$$K_{II} = c_{21}k_1 a^{\frac{1}{2}-\lambda_1} + c_{22}k_2 a^{\frac{1}{2}-\lambda_2} \tag{10b}$$

where c_{11}, c_{12}, c_{21}, and c_{22} are four dimensionless constants.

We calculate K_I and K_{II} as a function of the crack length by using the finite element method (Fig. 5a). We normalize K_I and K_{II} by $(G_\infty E')^{1/2}$. When $a/h << 1$, $K_I/(G_\infty E')^{1/2}$ and $K_{II}/(G_\infty E')^{1/2}$ are comparable. As a/h increases to one, $K_I/(G_\infty E')^{1/2}$ approaches one and $K_{II}/(G_\infty E')^{1/2}$ vanishes, signifying a return to mode I condition.

Recall $G = (K_I^2 + K_{II}^2)/E'$ (Irwin, 1957). By substituting Eq. (10), we obtain that

$$G = G_\infty\left[A_1\left(\frac{a}{h}\right)^{1-2\lambda_1} + A_2\left(\frac{a}{h}\right)^{1-\lambda_1-\lambda_2} + A_3\left(\frac{a}{h}\right)^{1-2\lambda_2}\right] \tag{11}$$

where

$$A_1 = \kappa_1^2(c_{11}^2 + c_{21}^2), \tag{12a}$$

$$A_2 = 2\kappa_1\kappa_2(c_{11}c_{12} + c_{21}c_{22}), \tag{12b}$$

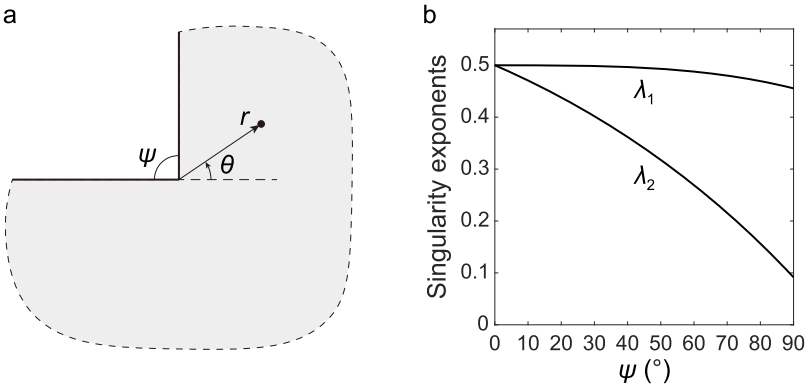

Fig. 4. Split singularities at a corner. (a) A corner in a homogeneous and linear elastic body. (b) Singularity exponents as a function of the angle of the corner, ψ.

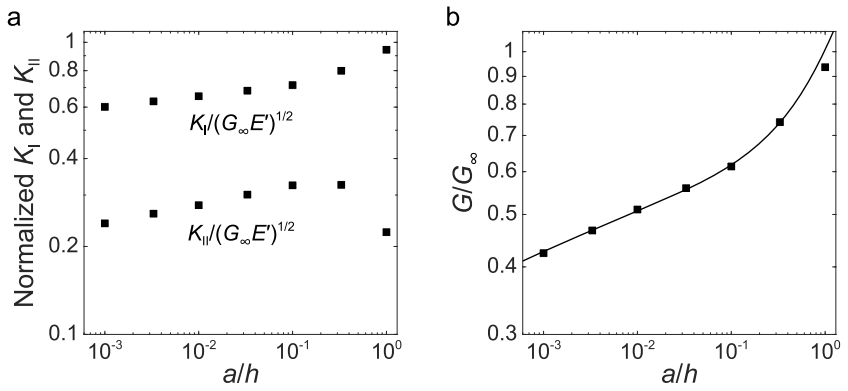

Fig. 5. The short-crack limit. (a) Stress intensity factors of the crack as functions of crack length. (b) Energy release rate as a function of crack length. Squares are data from the finite element calculation. The curve fits Eq. (11) to finite element data.

$$A_3 = \kappa_2^2\left(c_{12}^2 + c_{22}^2\right). \tag{12c}$$

For a chip corner with $\psi = 90^\circ$, $\lambda_1 = 0.45552$ and $\lambda_2 = 0.09147$ (Fig. 4b). When $a/h < 0.1$, we fit Eq. (11) to finite element data and obtain that $A_1 = 0.8167$, $A_2 = -0.3862$, and $A_3 = 0.5781$ (Fig. 5b). When $a/h > 0.1$, Eq. (11) does not fit well, indicating the crack is out of the influence by the corner.

When the crack length is large compared to the chip thickness, $a >> h$, the local energy release rate equals the global energy release rate $G = G_\infty$. That is, $f(\infty) = 1$. Given the short-crack and long crack limits, we find that the prefactor of the energy release rate for a crack of arbitrary length fits the relation (Fig. 6):

$$f\left(\frac{a}{h}\right) = \left\{1 + \left[A_1\left(\frac{a}{h}\right)^{1-2\lambda_1} + A_2\left(\frac{a}{h}\right)^{1-\lambda_1-\lambda_2} + A_3\left(\frac{a}{h}\right)^{1-2\lambda_2}\right]^{-\alpha}\right\}^{-\frac{1}{\alpha}}, \tag{13}$$

where $\alpha = 10.055$.

5. Conditions of crack initiation and arrest

Given an applied displacement Δ, the modulus E', the chip thickness h, the beam thickness H, the initial non-bonded beam length b_0, and the machine compliance c_m, Eqs. (6), (7), and (13) together define the G-a curve.

The conditions of crack initiation (Eq. (1)) and crack arrest (Eq. (2)) lead to an equation,

$$G\left(\Delta_c, a_{flaw}\right) = G(\Delta_c, a_{arrest}) \tag{14}$$

This equation corresponds to a horizontal line that intersects the G-a curve (Fig. 2). We combine Eqs. (6), (7), (13), and (14) in the form

$$\frac{a_{arrest}}{h} = F\left(\frac{a_{flaw}}{h}, c_m, \frac{b_0}{H}\right). \tag{15}$$

Here F is a dimensionless function of the three variables as indicated. This equation determines the crack length at which the crack

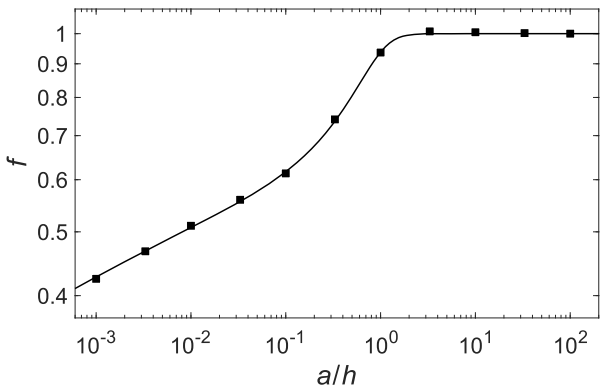

Fig. 6. Dimensionless function $f(a/h)$. Squares represent results computed by the finite element method and the curve fits Eq. (13).

arrests. We next describe the effects of the flaw size, the machine compliance, and the initial non-bonded beam length.

5.1. Effect of machine compliance

We plot G-a curves at various values of the machine compliance c_m (Fig. 7a). We normalize the local energy release rate G by the initial global energy release rate $G_\infty(b_0)$. For this plot, we fix the initial non-bonded beam length at $b_0/H = 10$. When the crack is short, the machine compliance does not affect the normalized G-a curves, and the G-a curves overlap. When the crack is long, the machine compliance increases the normalized local energy release rate. We plot a vertical dashed line to mark a value of the flaw size and intersect the G-a curve at a point, and then plot a horizontal dashed line that passes the point and intersects the G-a curve at another point. The left point indicates the crack initiation, whereas the right point indicates the crack arrest. Because the G-a curve is narrow at the top and is wide at the bottom, when the left point moves right, the right point moves left. Consequently, a larger flaw size leads to a smaller crack length at which the crack arrests. In experiments, although the flaw size is not controlled, the chip thickness may be reduced to increase the normalized value of the flaw size. We then compare various G-a curves: the left point is almost the same for each curve, but the right point differs from curve to curve. A large machine compliance leads to a large crack length at which the crack arrests. In experiments, we need a rigid machine and a narrow specimen so that the normalized value of the machine compliance $c_m = C_m E' W/8$ is small.

We then plot the crack length at which the crack arrests, a_{arrest}/h, as a function of the flaw size a_{flaw}/h, at various values of the machine compliance (Fig. 7b). The crack length at which the crack arrests decreases with the flaw size and increases with the machine compliance. The quantitative relationships align with the analysis presented above.

5.2. Effect of initial non-bonded beam length

We next plot G-a curves (Fig. 8a) and a_{arrest}-a_{flaw} curves (Fig. 8b) at various values of the initial non-bonded beam length b_0/H. For this plot, we fix the machine compliance at $c_m = 0$. How the initial non-bonded beam length affects the local energy release rate and the crack length at which the crack arrests is similar to that of the machine compliance. In experiments, we need a short initial non-bonded beam and a thick beam so that the normalized value of initial non-bonded beam length is small.

To guide experiments, we plot contours of the crack length at which the crack arrests a_{arrest}/h on the plane with the machine compliance c_m and the initial non-bonded beam length b_0/H as axes (Fig. 9). For this plot, we fix the flaw size at a_{flaw}/h=0.001. The contours allow us to check known experimental parameters and assess whether the crack length at which the crack arrests is smaller than the chip length. Interestingly, we find that for a fixed value of the machine compliance, the crack length at which the crack arrest does not always increase with the initial non-bonded length monotonically. For example, we plot a horizontal dashed line in Fig. 9, indicating a fixed machine compliance. The dashed line intersects the contours of a_{arrest}/h at multiple points. From the left to the right point, the corresponding values of a_{arrest}/h first decrease and then increase.

For a tensile tester with a certain value of the machine compliance c_m, an optimum value of initial non-bonded beam length b_0/H exists to minimize the crack length at which the crack arrests a_{arrest}/h. We plot a_{arrest}/h-b_0/H curves for various values of the machine compliance (Fig. 10a). For each curve, a_{arrest}/h decreases, reaches the minimum, and increases with b_0/H, except when c_m is negligible. Both the optimum value of b_0/H (Fig. 10b) and the minimum value of a_{arrest}/h (Fig. 10c) increase with c_m. For a given value of c_m, by comparing the minimum value of a_{arrest}/h to l_{chip}/h, we can assess whether the crack initiated from one corner of the chip can arrest before running to the other corner of the chip.

The flaw at the corner of a chip may have random shape, orientation, or position. When the double cantilever beam is pulled, the flaw can initiate an interfacial crack. Our model represents the flaw by a small interfacial crack of length a_{flaw}. The length of the flaw is a random variable, which may be used to characterize the quality of the fabrication process. The length of the flaw determines the peak force in the force-displacement curve (Fig. 1b). Conversely, the flaw size can be deduced from the peak force. In Eq. (11), set $G = G_c$,

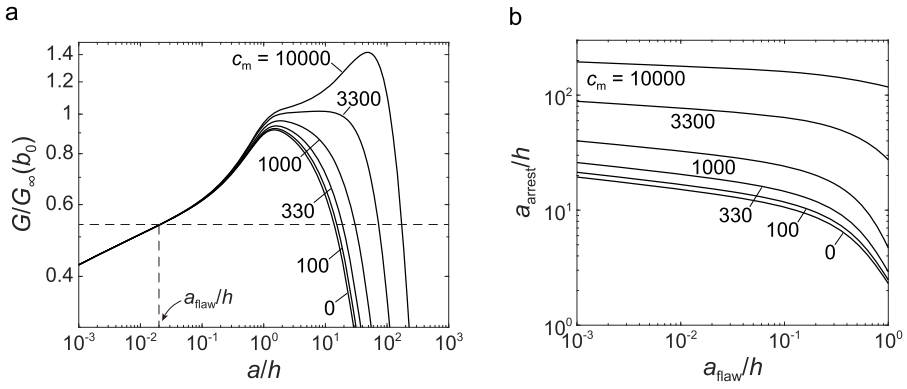

Fig. 7. Effect of machine compliance. (a) G-a curves and (b) a_{arrest}-a_{flaw} curves for various values of the machine compliance c_m. The initial non-bonded beam length is set to be $b_0/H = 10$.

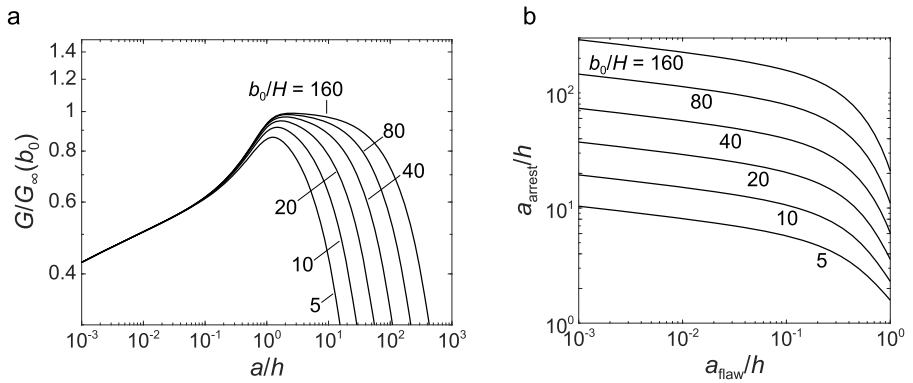

Fig. 8. Effect of initial non-bonded beam length. (a) G-a curves and (b) a_{arrest}-a_{flaw} curves for various values of the initial non-bonded beam length b_0/H. The machine compliance is set to be $c_m = 0$.

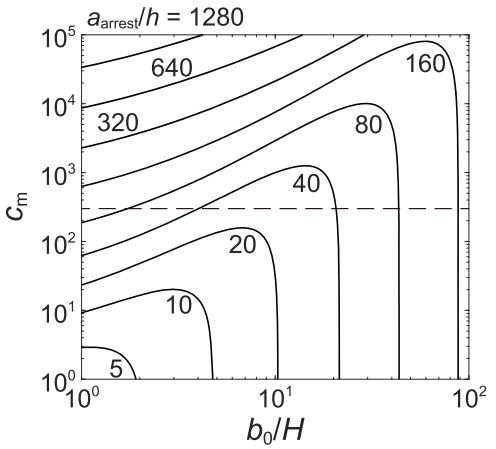

Fig. 9. Contours of crack length at which the crack arrests a_{arrest}/h on the plane with the machine compliance c_m and the initial non-bonded beam length b_0/H as axes. The flaw size is set to be $a_{flaw}/h = 0.001$.

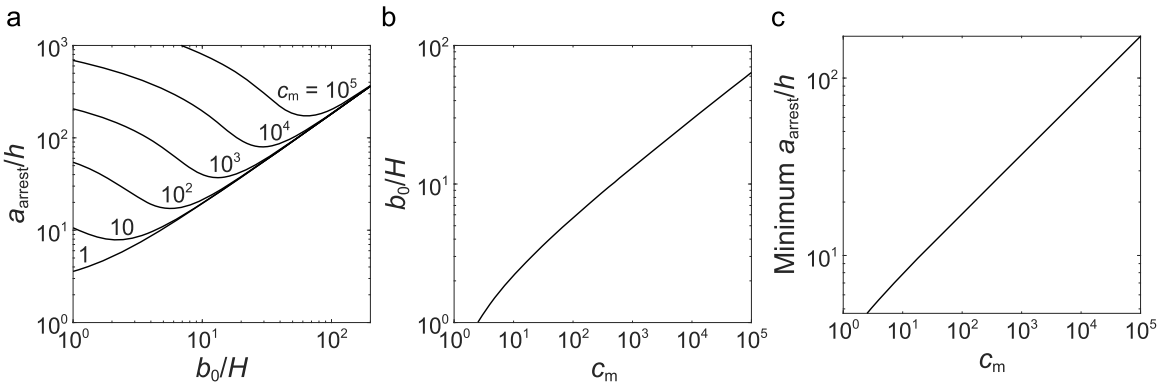

Fig. 10. Minimum crack length at which the crack arrests. (a) The crack length at which the crack arrests a_{arrest}/h as a function of the initial non-bonded beam length b_0/H for various values of the machine compliance c_m. (b) Optimum value of b_0/H as a function of c_m. (c) Minimum a_{arrest}/h as a function of c_m. The flaw size is set to be $a_{flaw}/h = 0.001$.

and calculate G_∞ using Eq. (3) along with the experimentally measured peak force.

6. Concluding remarks

We have studied the initiation and arrest of a crack from a corner in a multi-chip semiconductor device using a double cantilever beam that sandwiches a row of chips. The crack initiates from the corner, runs unstably on the interface, and may or may not arrest. The unstable growth of the crack, as well as possible arrest, originates from the non-monotonic relation between the energy release rate and the crack length. We compute the energy release rate and relate the conditions of crack initiation and arrest to the machine compliance, the specimen geometry, and the flaw size. The force that initiates the crack can be used to estimate the initial flaw size at the corner. If the crack arrests, subsequent increase of the applied displacement will drive the crack to grow further stably. This stable crack growth can be used to determine toughness. We hope that this study will aid the development of emerging architectures of semiconductor devices.

CRediT authorship contribution statement

Guodong Nian: Writing – review & editing, Writing – original draft, Methodology, Investigation, Formal analysis, Conceptualization. **Yu-Sheng Lin:** Investigation. **Jia-Ming Yang:** Investigation. **Sammy Hassan:** Writing – review & editing. **Jyun-Lin Wu:** Investigation. **Sherwin Tang:** Investigation. **Jun He:** Funding acquisition. **Joost J. Vlassak:** Writing – review & editing, Supervision. **Zhigang Suo:** Writing – review & editing, Writing – original draft, Supervision, Funding acquisition, Conceptualization.

Declaration of competing interest

The authors declare no competing interest.

Data availability

Data will be made available on request.

Acknowledgment

The work at Harvard was supported by a contract from TSMC. The paper was submitted to a special issue of Journal of the Mechanics and Physics of Solids in honor of Professor Huajian Gao on the occasion of his sixtieth birthday.

References

Blackman, B., Kinloch, A., 2001. Fracture tests on structural adhesive joints. European Structural Integrity Society. Elsevier, pp. 225–267. https://doi.org/10.1016/S1566-1369(01)80036-4.

Chen, C.-P., Chen, Y., Subbarayan, G., 2021. Singular enrichment for multi-material corners with application to assessing the risk of fracture in semiconductor devices. Eng. Fract. Mech. 248, 107739 https://doi.org/10.1016/j.engfracmech.2021.107739.

Irwin, G.R., 1957. Analysis of stresses and strains near the end of a crack traversing a plate. J. Appl. Mech. 24, 361–364. https://doi.org/10.1115/1.4011547.

Lau, J.H., 2022. Recent advances and trends in advanced packaging. IEEE Trans. Compon. Packag. Manuf. Technol. 12, 228–252. https://doi.org/10.1109/TCPMT.2022.3144461.

Liu, X.H., Suo, Z., Ma, Q., 1999. Split singularities: stress field near the edge of a silicon die on a polymer substrate. Acta Mater 47, 67–76. https://doi.org/10.1016/S1359-6454(98)00345-0.

Lu, R., Chuang, Y.-C., Wu, J.-L., He, J., 2023. Reliability challenges from 2.5D to 3DIC in advanced package development. In: 2023 IEEE International Reliability Physics Symposium (IRPS). Presented at the 2023 IEEE International Reliability Physics Symposium (IRPS). IEEE, Monterey, CA, USA, pp. 1–4. https://doi.org/10.1109/IRPS48203.2023.10117647.

Rabie, M.A., Polomoff, N.A., Pozder, S., 2021. Optimizing die corner and optical groove corner crackstop support structures for mitigating dicing and CPI risks. In: 2021 IEEE 71st Electronic Components and Technology Conference (ECTC). Presented at the 2021 IEEE 71st Electronic Components and Technology Conference (ECTC). IEEE, San Diego, CA, USA, pp. 1391–1398. https://doi.org/10.1109/ECTC32696.2021.00223.

Rivlin, R.S., Thomas, A.G., 1953. Rupture of rubber. I. Characteristic energy for tearing. J. Polym. Sci. 10, 291–318. https://doi.org/10.1002/pol.1953.120100303.

Wiederhorn, S.M., Shorb, A.M., Moses, R.L., 1968. Critical analysis of the theory of the double cantilever method of measuring fracture-surface energies. J. Appl. Phys. 39, 1569–1572. https://doi.org/10.1063/1.1656397.

Williams, M.L., 1952. Stress singularities resulting from various boundary conditions in angular corners of plates in extension. J. Appl. Mech. 19, 526–528. https://doi.org/10.1115/1.4010553.